High-Speed OH-PLIF Diagnostics of Flame Flashback in Low Swirl Hydrogen-Enriched Flames

Pradeep Parajuli[1, 2]; Peter Strakey[1]

[1]National Energy Technology Laboratory, 3610 Collins Ferry Road, Morgantown, WV 26505, USA

[2]NETL Support Contractor, 3610 Collins Ferry Road, Morgantown, WV 26505, USA

ABSTRACT

Hydrogen-enrichment is a potential strategy to reduce carbon emissions for the development of next-generation lean premixed combustors. However, the higher flashback propensity with hydrogen enrichment owing to the faster chemical kinetics is one of the key challenges in existing natural gas turbine combustors. The fundamentals of stabilized flame dynamics and flashback events in a premixed low swirl burner (LSB) configuration are visualized experimentally using nanosecond (ns)-based high-speed hydroxyl radical planar laser-induced fluorescence (OH-PLIF). The LSB burner has an optically accessible pre-mixing tube allowing laser diagnostic investigation of flashback events. Swirlers with two different turning angles, 26° and 33° and three different center-body hole diameters, 1.08, 1.12, and 1.16 mm with measured swirl numbers varying from 0.43 to 0.49 are tested in this study at atmospheric temperature and pressure inlet conditions. The inlet conditions are varied systematically with respect to pre-mixer velocities (V), flame equivalence ratio (ϕ), and hydrogen content (X_{H_2}) for 50%-90% (H_2, by mole) H_2/CH_4 reactant mixtures and OH-PLIF characterization is performed in a stable flame at 20 kHz repetition rate. An increase in flashback propensity is observed with increasing ϕ, X_{H_2} and decreasing V via detailed investigation of flame lift-off length (L) above the burner rim. Flashback ϕ (ϕ_{FB}) investigations show an expected linearly increasing trend with decreasing X_{H_2} and increasing V for each swirler studied and the results agree well with detailed L investigations in a stable flame configuration. ϕ_{FB} studies for different swirlers show an increase in flashback resistance with the increase in center-body hole diameter and swirl angle. High-speed OH-PLIF images recorded at a 1 kHz repetition rate depict flashback initiation, flashback to flame holding transition and flame anchoring between the swirling and non-swirling regions of the LSB. Spatiotemporally resolved kHz-rate OH-PLIF is a promising technique to observe rapidly occurring flashback events and it can be applied for turbulence-chemistry interaction model validation.

INTRODUCTION

Hydrogen and hydrogen-enriched fuels are considered a clean and sustainable energy source and are the key enabler of the energy transition to replace conventional fuels for the development of next-generation gas turbine engines [1-4]. The use of hydrogen-enriched fuels can significantly reduce the production of carbon-based products in the power generation industry. However, high-hydrogen flames are particularly susceptible to flashback which is one of the key issues in retrofitting lean-premixed natural gas turbine combustors. Flashback events occur when the flame front propagates upstream from the combustor into the premixer section. Such events can cause catastrophic failure of the combustor as the pre-mixing tubes are not designed to handle a high heat load. The propensity for flashback increases with an increase in hydrogen content of the reactant mixture due to the faster chemical kinetics and smaller quenching lengths of hydrogen-rich flames [5].

The successful design of next-generation gas turbine engine combustors requires a better fundamental understanding of flashback events. Currently, most gas turbine combustors include a swirling flow for flame stabilization and mixing processes which requires a detailed study of flashback events. Swirl-stabilized flame methods are essential to lean-premixed combustion systems because of their significant benefits such as an increase in flame intensity and stability, as well as combustor performance [6]. Low swirl burners (LSBs) have gained increasing attention since they were originally developed by Cheng [7] for fundamental studies. LSBs have a non-swirling core surrounded by a swirling shroud and utilize a flow divergence concept allowing the flame to freely propagate and stabilize at a position where the local flow velocity is equal and opposite to the flame speed [8]. Flashback becomes likely to occur if the bulk flow velocity is reduced further as the velocity at the burner exit is close to the flame speed. Avoidance of such flashback events is critical to the design of hydrogen-safe gas turbine combustors; however, the lack of relevant fundamental knowledge of flashback modes in LSBs and their underlying mechanism remains a major obstacle.

In this study, the flashback mechanism in low swirl flames is investigated in an optically accessible LSB via the visualization of spatiotemporally resolved hydroxyl (OH) radicals using Planar Laser-Induced Fluorescence (PLIF). This study is an extension of previous work conducted at the National Energy Technology Laboratory (NETL) [9]. In the next section, a brief description of the optically accessible LSB, high-speed pulsed laser, and detection system are presented. Section 3 presents a series of single-laser-shot OH-PLIF images recorded while the LSB is operated under flashback mode. The detailed investigation of different inlet mixture parameters on burner equivalence ratio at flashback are studied and outlined.

EXPERIMENTAL APPARATUS

The experimental setup used for these measurements consists of an optically accessible laboratory-scaled swirl-stabilized burner, high-repetition rate ns-pulsed laser system, high-speed detection system, and is displayed schematically in Figure 1.

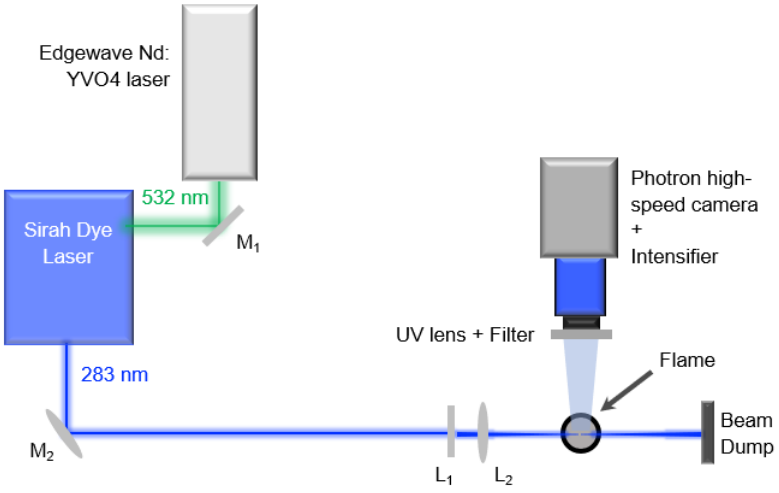

Figure 1: Schematic diagram of the experimental apparatus for OH-PLIF imaging in a LSB (M_1: 532 nm mirror; M_2: 284 nm mirror; L_1 & L_2: sheet-forming optics).

A. Burner Configuration

The burner facility consists of fuel (H_2 and CH_4) and air sources, mass flow controllers, flashback and flame management sensors and solenoid valves, a flow straightener, swirlers, and optically accessible pre-mixer assembly. A mixture of CH_4 gas with varied percentages of H_2 gas is premixed with air and is fed into a flow straightener to minimize the lateral velocity of the reactant mixture. The mixture then enters the swirler which creates recirculation zones, enhancing the fuel-air mixing and flame stabilization process. The burner system used in this study is the same as that used by Searle et al. [9] during previous flashback studies except the burner was modified to provide optical access in the pre-mixing section to visualize flashback dynamics. A 21.2-mm inner diameter and optically accessible pre-mixer assembly utilized in the present study is shown in Figure 2a. The pre-mixer tube is sliced by a plane parallel to its axis to fit an optical window for laser sheet and imaging access. The optical window was fabricated using a clear fused quartz tube with a section cut out to fit into the pre-mixer tube. A thermocouple is inserted into the premixing section of the burner via a tiny port just above the swirler to detect the flashback when it occurs.

The swirler is the most important component of this burner and its design is depicted in Figure 2b. The swirler was additively manufactured from 316 stainless steel using laser powder bed fusion. The air/fuel mixture through the central channel remains straight while that through the swirler vanes impart swirling motion to the annular flow promoting the flow divergence. A perforated plate is attached to the center channel which breaks down the large turbulent structures and balances the pressure drop across central and annular regions. The more flow is blocked by the central perforated region, the more flow passes through the annular region of the swirler. The design dimensions for swirler, perforated plate, and optical window are provided in Table 1. Briefly, it has an injector radius of 10.4 mm, and 16 curved swirler vanes of thickness 0.75 mm. The swirler angle, α, and perforated plates hole diameter, d, are varied to achieve measured swirl numbers between 0.43 to 0.49. Such small range in swirl numbers are optimal to investigate LSB performance [8]. The radius ratio (R), defined by a ratio of center-body outer radius to injector radius is kept constant at 0.65. The perforated plate fitted to the LSB in Figure 2 has 25 equal-sized holes (1.08 mm, 1.12 mm, and 1.16 mm in diameter) arranged in a circular grid to give 78.3%, 76.7%, and 75% blockage, respectively, regulating the axial mass flow rate through the center channel. The swirler is recessed from the burner tube exit into the pre-mixer section by 27 mm and it is essential to produce lift-off flames.

Table 1: Design parameters for swirler, perforated plate and optical window.

Swirler	**Unit**	**Value**
Injector radius (R_i)	mm	10.4
Center-body outer radius (R_c)	mm	6.8
Radius ratio (R)	-	0.65
Center-body axial length (l_c)	mm	16
Center-body wall thickness (t_c)	mm	1
Swirler angle (α)	degree	26 and 33
Number of vanes (n)	-	16
Vane axial length (l_v)	mm	12
Vane thickness (t_v)	mm	0.75
Perforated plate	**Unit**	**Value**
Thickness (t)	mm	1
Hole diameter (d)	mm	1.08, 1.12 and 1.16
Number of holes (n_{holes})	-	25

Hole to burner diameter ($d/2R_i$)	-	0.058
Optical window	**Unit**	**Value**
Inner diameter (*ID*)	mm	22
Outer diameter (*OD*)	mm	25
Window length (*l*)	mm	63.5

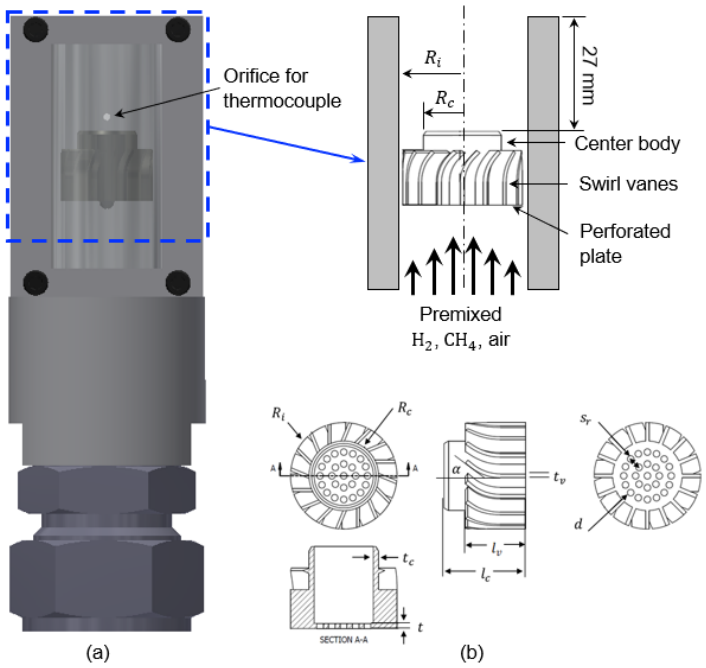

Figure 2: Design of (a) optically accessible pre-mixer system (b) swirler used in the present study.

B. Laser System and Imaging Apparatuses

The laser diagnostics system for OH-PLIF imaging consists of a ns-duration Nd:YVO4 laser (INNOSLAB, Model: IS400-2-L) operating at 1,064-nm wavelength. The frequency-doubled output laser beam at 532 nm wavelength with an input power of ~110 W at 20 kilohertz (kHz) and a unique 3 mm x 8 mm rectangular beam profile is used to pump a frequency-tunable dye laser (Sirah, Model: CREDO-DYE-N). The dye laser includes a high flow rate dye cell filled with a solution of rhodamine-6G dye diluted in pure ethanol which allows efficient production of a ~566 nm beam. The laser beam is frequency doubled in a nonlinear crystal to generate ultraviolet (UV) radiation near 284 nm wavelength and is isolated from the fundamental beam using a wavelength separation unit. The UV beam is guided into the probe region using a 45° mirror and a combination of cylindrical and spherical lenses to generate a beam sheet of approximately 30 mm height to excite the OH $A^2\Sigma^+$-$X^2\Pi$ (1,0) band. The OH-PLIF signal is collected perpendicular to the direction of the propagation of the laser beam sheet using a high-speed intensifier (Invisible Vision, Model: UVi 1850-10 S25) coupled to a high-speed CMOS camera (Photron, Model: FASTCAM SA-Z). An appropriate set of filters is mounted in front of the detection system to collect strong OH fluorescence emissions near 309 nm and block unwanted chemiluminescence interference and laser scattering.

RESULTS AND DISCUSSIONS

The burner was operated in two different configurations to characterize stable flames and flame flashback. The initial temperature and pressure of the gaseous mixture were set at 298 K and 1 atm, respectively. Before the test, the dependence of the OH-PLIF signal on the excitation wavelength was recorded in an atmospheric pressure 10%H_2/90%CH_4-air flame at $\phi = 0.7$. The laser wavelength was scanned within the ±1-nm range at approximately 283.5 nm, observing the OH-PLIF signal to find the peak excitation wavelength. As expected, the optimized excitation wavelength was found to be 283.9 nm, confirmed by the OH signal excitation spectrum obtained from LIFBASE [10]. Also, the OH-PLIF signal shows no apparent deviation from the expected linear dependence (owing to single-photon excitation) for the range of laser energy scanned, suggesting no saturation effect and hence the laser energy was held constant at ~ 0.05 mJ/pulse for the remaining experiments.

A. Characterization of Low Swirl Stabilized Flame

Effect of Inlet Pre-Mixer Velocity

To investigate the high-hydrogen flame dynamics, the OH-PLIF signal was recorded as a function of inlet pre-mixer velocity (V) from 5 m/s to 10 m/s at 20 kHz-repetition-rate. Several single-laser-shot OH-PLIF images were acquired and 500 such individual frames were averaged together to analyze OH-PLIF variation and L during post-processing. L was measured as the distance from the burner rim to the base of the lifted flame. Figure 3 shows the effect of V on the averaged OH-PLIF signal and L. Each OH signal data point is obtained by integrating the entire region of the averaged flame. As expected, the OH signal shows a negligible variation with V; however, L tends to increase linearly with it. This linear increase in the L effect is created by higher inlet velocities which push the combustion zone further downstream. A similar effect on gaseous fuel combustion with the jet velocity were observed and predicted previously in the literature [11-14]. This shows that as the local gas velocity is increased compared to the flame speed, the risk of flashback is minimized. Quantitatively, L increases from 1 mm above the burner to approximately 6 mm when the velocity is increased from 5.5 m/s to 10 m/s.

A series of spatially resolved representative background-corrected OH-PLIF images recorded for 70%H_2/30%CH_4-air flame is illustrated in Figure 4. The horizontal axis represents the radial distance in "mm" with zero indicating the axis of the burner tube. Similarly, the vertical axis represents the height above the burner (HAB) in "mm." The bright area represents the spatially resolved OH-PLIF signal in the combustion flame zone. Subsequently, the dark region directly downstream of the burner outlet represents the unburnt mixture of fuel and oxidizer as well as ambient air. The sharp OH-PLIF signal gradient is observed along the upstream edge of the OH signal which marks down the upstream flame front and the signal decays quickly beyond the flame front when it mixes with the atmospheric air. The decay of the OH-PLIF signal in the downstream direction is attributed to the relaxation of super-adiabatic OH flame-front concentrations back to equilibrium levels. Furthermore, this series of high-speed OH-PLIF images clearly depict the formation of isolated hot pockets, their growth, breakage and merging into the main flame region, along with several other complex flame features, local ignition, and local extinction. Considering these OH-PLIF images provide the relative burning intensity, a quantitative evaluation of OH concentration is not performed. The increase in L is evident when V is increased from 5.5 m/s (top row) to 10 m/s (bottom row). The increase in V leads to an increase in combustion instability and flame fluctuations effect [15] as shown in Figure 4.

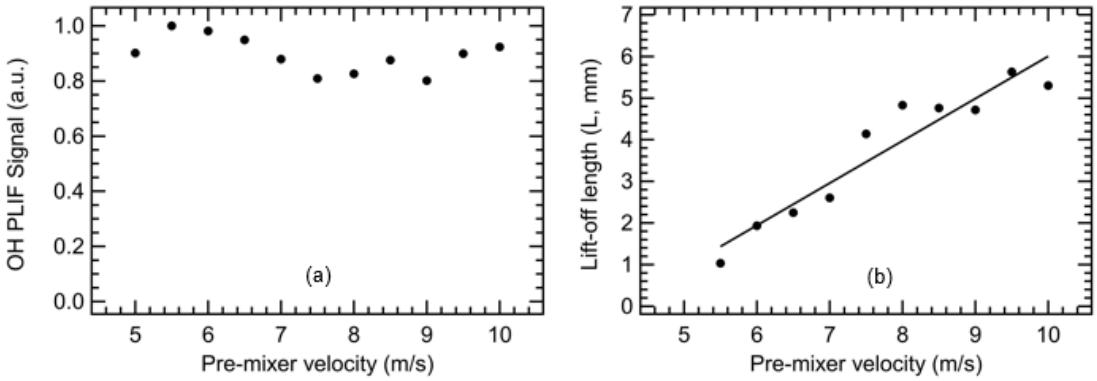

Figure 3: (a) Variation of OH-PLIF signal as a function of V for 70%H_2/30%CH_4-air flame at ϕ = 0.4. (b) L as a function of V for 70%H_2/30%CH_4-air flame at ϕ = 0.4.

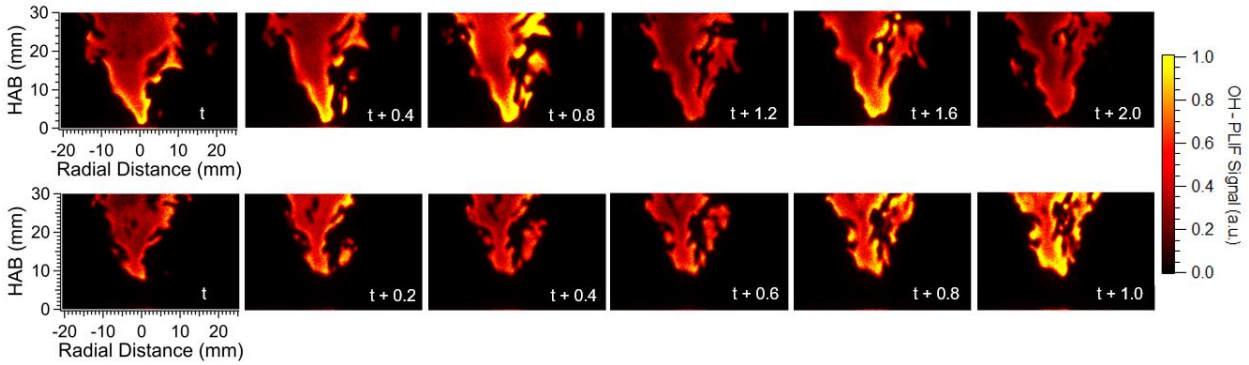

Figure 4: Sequence of single-laser shot OH-PLIF images showing flame dynamics for 70%H_2/30%CH_4-air flame at ϕ = 0.4 and V of 5.5 m/s (top row) and 10 m/s (bottom row). The time stamp for the occurrence of each event is shown on the bottom right corner of each frame in milliseconds (ms).

Effect of Hydrogen Content

Shown in Figure 5 is the dependence of the OH-PLIF signal and L on the hydrogen content (X_{H_2}) in the reactant mixture. The Φ and V were kept constant at 0.4 and 7.5 m/s, respectively. It is observed that a higher X_{H_2} in the reactant mixture also increases the OH concentration. The increase in OH concentration also relates to an increase in flame temperature which is expected as a hydrogen flame is hotter than a methane flame at the same ϕ. The equilibrium temperature calculated using the STANJAN chemical equilibrium calculator is also included in the plot which shows an increase of 80 K temperature when X_{H_2} increased from 50% to 90%. A similar effect of the X_{H_2} on OH signal was observed by Yang et al. [16] while investigating syngas/air-premixed turbulent flame combustion. A detailed study of the effect of X_{H_2} on L revealed that increasing the X_{H_2} in the mixture tends to decrease L and increases the chances of flashback in the hydrogen-enriched flame. When compared to the V, L in hydrogen-enriched flame is more sensitive to the X_{H_2} in the reactant mixture supporting the claim made by Liu et al. [14]. As X_{H_2} is increased in the reactant mixture for a fixed velocity and ϕ, the L of the flame decreased nonlinearly with the increasing X_{H_2}. The decrease in L is faster at low X_{H_2} when compared to high X_{H_2} flames. A similar nonlinear decrease owing to the changes in autoignition delay time and flame speed was also observed by

Liu et al. [14] during an OH* chemiluminescence study in hydrogen auto-ignited flames. A sudden rise in the flame speed (S_L) is observed when X_{H_2} is increased above 70% in hydrogen-enriched flame as depicted in Figure 5c. The increase in hydrogen induced a higher turbulent flame speed and more dynamic features like wrinkling, flame breakages, and an increase in flame width. These ultrafast flame dynamics are spatiotemporally resolved and are highlighted in Figure 6.

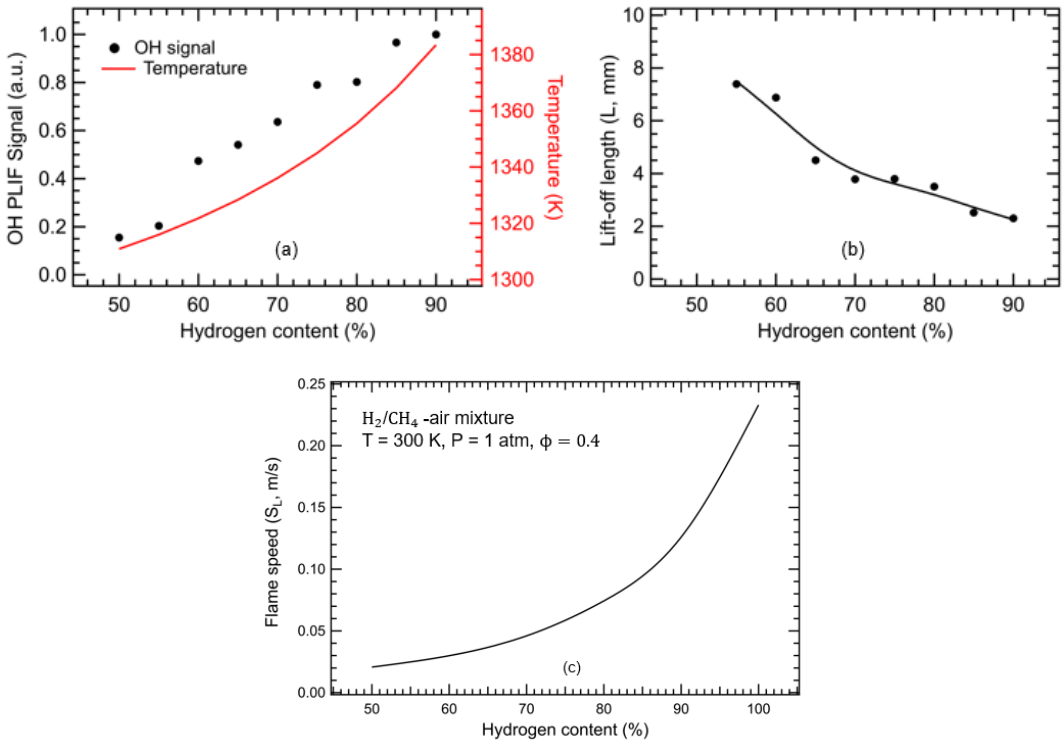

Figure 5: (a) Variation of OH-PLIF signal and equilibrium flame temperature as a function of X_{H_2} in the reactant mixture with V= 10 m/s and ϕ = 0.4. (b) L as a function of X_{H_2} in the reactant mixture at V= 7.5 m/s and ϕ = 0.4. (c) Variation of S_L as a function of X_{H_2} in the reactant mixture at ϕ = 0.4.

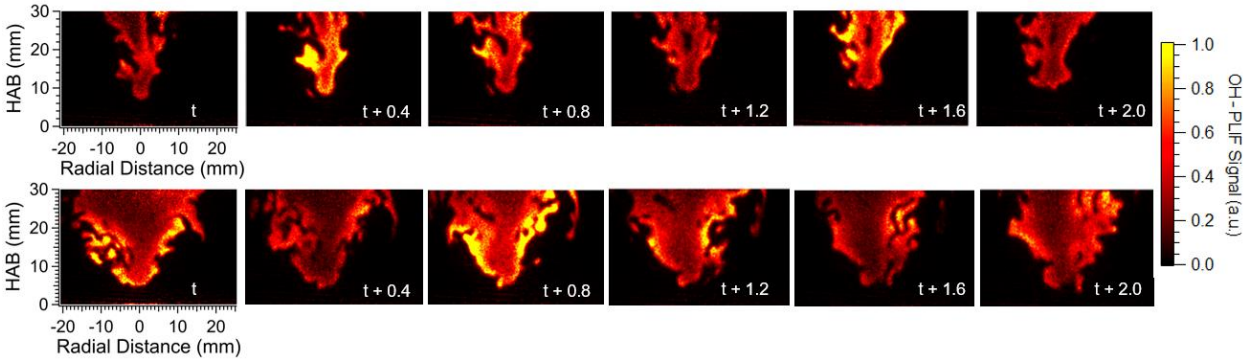

Figure 6: Sequence of single-laser shot OH-PLIF images showing flame dynamics at ϕ = 0.4 and V of 7.5 m/s for 60%H_2/40%CH_4-air flame (top row) and 85%H_2/15%CH_4-air flame (bottom row). The time stamp for the occurrence of each event is shown on the bottom right corner of each frame in ms.

Effect of Equivalence Ratio

The OH-PLIF diagnostic was applied to measure the experimental OH radical signal as a function of ϕ in a 70%H_2/30%CH_4-air flame. The X_{H_2} and V were kept constant at 70% and 10 m/s, respectively. The corresponding OH-PLIF dependency on Φ is shown in Figure 7a. The general trend is OH radical concentration peaks at a stoichiometric condition and decays rapidly as the reactant mixture becomes leaner. A similar trend is observed experimentally where the OH-PLIF signal decays as ϕ is decreased from 0.60 to 0.35. In this study, ϕ was scanned in a narrow range of 0.35 to 0.60, limited by lean blowout condition and avoidance of flame flashback. Detailed study of ϕ on L revealed that increasing ϕ brings the flame closer to the burner surface increasing the risk of flashback due to increased flame speed. As ϕ is increased, the flames ultimately attach to the burner tube edge with uniform OH-intensity and local burning rates [6] and flashback then occurs once a threshold ϕ is reached. This decrease in L is evident in Figure 8 when ϕ is increased from 0.40 (top row) to 0.55 (bottom row). Six single-laser-shot frames each for the two ϕs studied are presented here. The dark regions represent either the unburnt fuel-air reactants or surrounding air depending on the location, while the bright red and yellowish portion indicates the presence of products. The light intensity of this portion has a direct relationship with OH radical concentration and the combustion intensity of the flame. It is observed that low OH radical concentration exists in the inner part of the flame zone. The flame front shows high OH concentration and is characterized by wrinkles especially in the top region and fluctuates from frame to frame. The increase in ϕ induced a higher turbulent flame speed and more dynamic features like wrinkling, flame breakages, and an increase in flame width as observed in Figure 8.

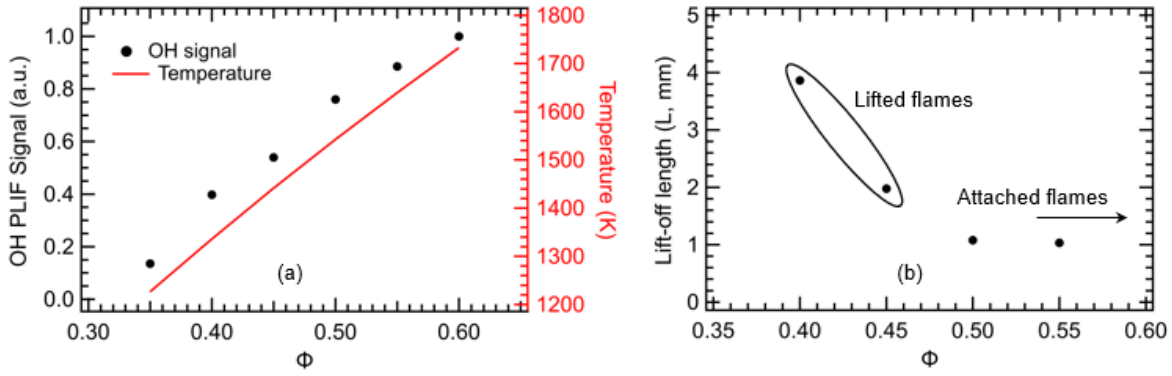

Figure 7: (a) Variation of OH-PLIF signal and equilibrium flame temperature as a function of ϕ for 70%H_2/30%CH_4-air flame at V = 10 m/s. (b) L as a function of ϕ for 70%H_2/30%CH_4-air flame at V = 7.5 m/s.

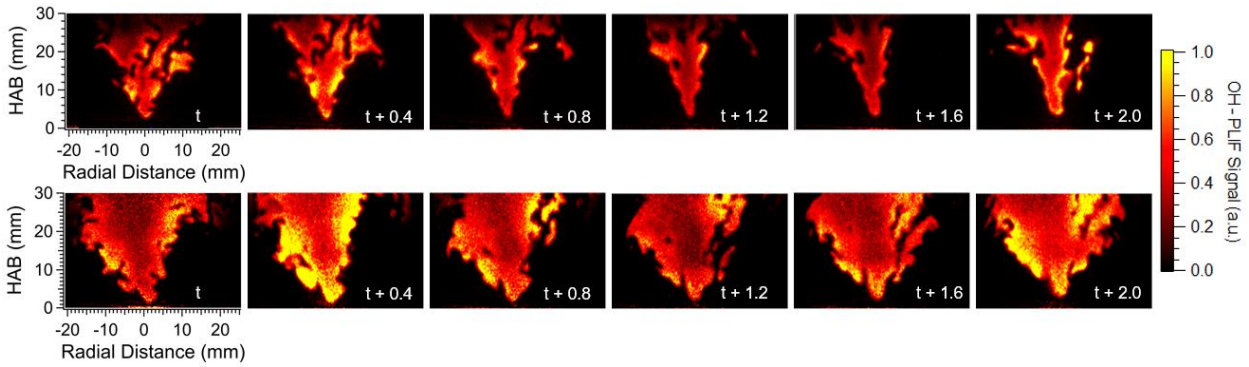

Figure 8: Sequence of single-laser shot OH-PLIF images showing flame dynamics for 70%H_2/30%CH_4-air flame at V of 7.5 m/s and ϕ = 0.4 (top row) and ϕ = 0.55 (bottom row). The time stamp for the occurrence of each event is shown on the bottom right corner of each frame in ms.

B. Investigation of Flame Flashback Events

Figure 9a shows the dependence of flashback equivalence ratio (ϕ_{FB}) on the proportion of X_{H_2} (60% to 90%) in reactant mixtures for three different V (5, 7.5, and 10 m/s). It is observed that at a constant V, ϕ_{FB} decreases linearly with an increase in X_{H_2} in the reactant mixture. As X_{H_2} increases in the H_2/CH_4-air mixture, the overall flame speed of the reactant mixture increases as mentioned earlier in Figure 5c [17-19], and the flame flashback is more likely to occur. This statement is further evidenced by the decrease in L as X_{H_2} increases, indicated in Figure 5b. As the V of the reactant mixture increases (keeping constant X_{H_2}), the flashback resistance of the burner system increases as the local fuel velocity grows large relative to the flame speed of the mixture. The dependence of ϕ_{FB} on the velocity at constant X_{H_2} was found to be linear as indicated in Figure 9b. The error bar for the V of 7.5 m/s for 70%H_2/30%CH_4-air flame represents a 2-sigma standard deviation of ϕ_{FB} obtained from six different experimental tests.

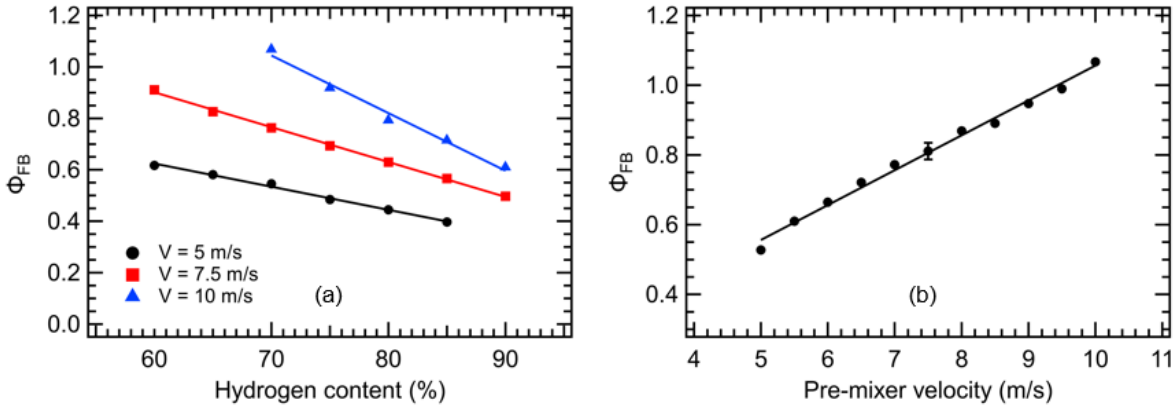

Figure 9: Dependence of ϕ_{FB} upon (a) X_{H_2} for three different Vs (5, 7.5, and 10 m/s) (b) V for 70%H_2/30%CH_4-air flame at reactants temperature 300 K and pressure 1 atm.

A series of spatially resolved representative OH-PLIF images recorded for a 65%H_2/35%CH_4-air flame is illustrated in Figure 10. The horizontal axis represents the radial distance in "mm" with zero indicating the axis of the burner tube. Similarly, the vertical axis represents the depth below the burner rim in "mm." The 9-mm width clips were used to hold the optical window into the burner and hence the region of interest during these flashback experiments lies 9 mm below the burner surface. The location of the swirler is shown in the bottom row images for better visualization of the location of flashback events. These images were recorded by keeping the V constant at 7.5 m/s and slowly increasing ϕ until the occurrence of flashback (whenever applicable). The $\frac{d\phi}{dt}$ defined by the change in ϕ with respect to time, t was set at 0.001, i.e., for each 1-s time interval, ϕ was increased by 0.001 and was dictated via the mass flow controllers. As ϕ is increased the flame speed increases compared to the local gas velocity and the flame becomes more susceptible to flashback. Once ϕ_{FB} is reached, the flame propagates further upstream into the pre-mixer tube until it reaches flame stabilization mode. The spatiotemporally resolved OH-PLIF images revealed the occurrence of flashback-to-flame holding transition within 30–40 ms of the entrance for all the fuel combinations tested during this study. At first, the flame tongue starts interacting with flammable mixtures

in the pre-mixing tube. The flame structures interact strongly with the fresh unburnt flow around it and appear to rapidly grow in size within a few milliseconds. These characteristics were observed in other flashback studies conducted in H_2-natural gas-air mixtures [20, 21]. In contrast, no bright appearances of such propagating structures and isolated hot pockets are observed in this study suggesting rather uniform mixing along the flame propagation path although additional study is required for verification.

As the propagating flame structures reach closer to the swirler they bifurcate into two leading tips (from a two-dimensional perspective). After a certain duration, these structures anchor inside the mixing tube just above the swirler on the rim of the center-body between the swirling and non-swirling regions of the LSB as depicted in the bottom row images. Once the flame anchors on the rim of the center-body, it does not move upstream but continues to interact with fresh unburnt reactants, fluctuating from frame-to-frame. Potential explanations for the sustained flame anchoring in the mixing tube could be: the continuous presence of fresh unburnt mixture inside the tube, heating of the inner wall of the mixing tube and rim of the center-body reducing quenching distance, and boundary layer separation taking place at the location of the flame tip [22]. The pre-mixer velocity used here is not high enough to blow off the flame from the rim of the center-body. The influences of the central non-swirling flow and annular swirling flow are clearly observed in the flame. The two V-shaped flame structures formed by the central jets and swirling flow are merged together in the downstream flow during the flame anchoring process forming a conical flame front just above the center-body. The flame front is characterized by wrinkles, especially in the top part and fluctuates from frame-to-frame as shown in Figure 10. It further illustrates that the height of the flame front decreases as X_{H_2} increases in the reactant mixture. Chen et al. [23] observed a similar effect of X_{H_2} on flame front height while investigating 0% to 50% hydrogen-fueled reactant mixtures but the study was conducted in a stable, laminar premixed liquified petroleum gas-hydrogen flame. This shorter flame front for increasing X_{H_2} is associated with the increase in the flame speed of the reactant mixture due to high X_{H_2}. As mentioned earlier, a thermocouple inserted into the pre-mixing section above the swirler senses the rise in temperature due to anchored flame and the incoming fuel is shut off. Approximately 300–500 ms of such flashback events and flame-holding transitions within the tube were captured before it extinguished.

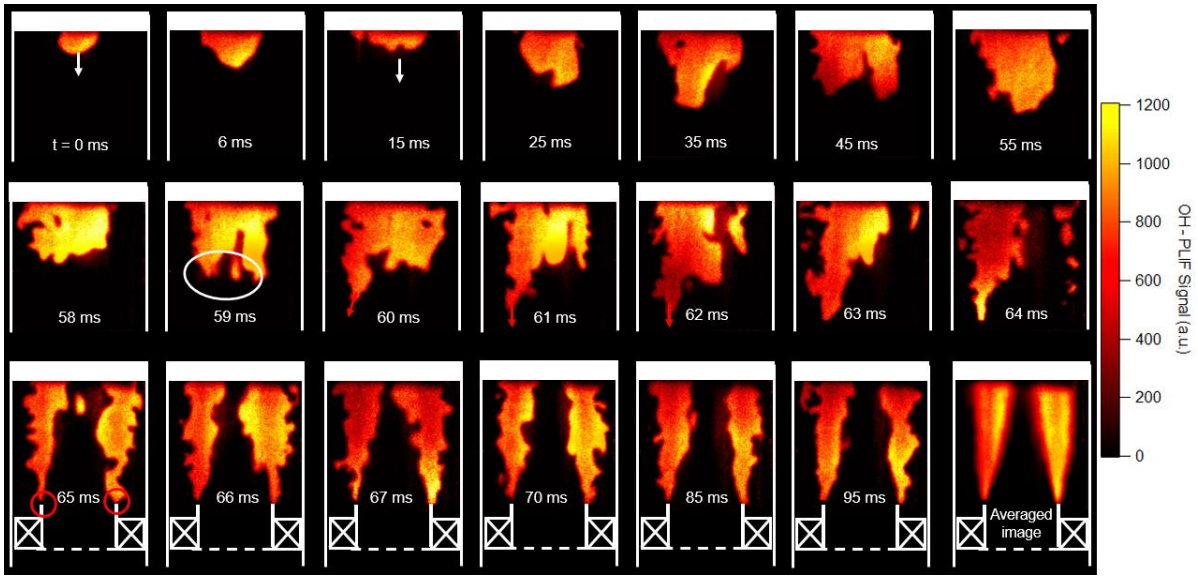

Figure 10: Sequence of single-laser shot OH-PLIF images showing temporal evolution of flame flashback events inside the pre-mixer tube for 60%H_2/40%CH_4-air flame at V = 7.5 m/s. Several

single-laser-shot OH-PLIF images were acquired visualizing the anchored flame and 200 such individual frames were averaged during post-processing and is depicted in bottom right corner.

Figure 11a shows the dependence of ϕ_{FB}on X_{H_2} for three different center-body hole diameter – 1.08, 1.12, and 1.16 mm creating blockage ratio (BR) of 0.783, 0.767, and 0.750 respectively. The swirl vane angle was kept constant at 33°. An increase in perforated plate hole diameter decreases the BR which increases the flow via the center-body and the burner system becomes less flashback prone, as depicted in Figure 11a. In other words, reducing the axial mass flow rate via center-body (by increasing BR), results in flame flashback. Another interesting observation is on the slope of the flashback lines which shows a greater negative slope with increasing d (or decreasing BR). This means for same amount of increase in X_{H_2}, the decrease in ϕ_{FB} is more for a higher d (or a lower BR). No flashback was observed at lower X_{H_2} for d = 1.16 mm at V = 7.5 m/s even when flame ϕ is ramped to 1. The error bars shown for few data points represent a 2-sigma standard deviation of ϕ_{FB} obtained from five different experimental tests. Figure 11b shows the dependence of ϕ_{FB}on X_{H_2} for two different swirl vane angles – 26° and 33° represented by black circle and blue triangles respectively. The center-body hole diameter was kept constant at 1.16 mm, creating a constant BR of 0.750. An increase in α increases the flashback resistance of the burner system at V = 7.5 m/s, as depicted in Figure 11b. This could be because the increasing swirling angle creates a stronger swirl flow which promotes rapid divergence near the burner exit allowing better flame stabilization. The slope of the flashback lines for α = 33° shows a greater negative slope when compared to flashback lines for α = 26°. The error bar represents a 2-sigma standard deviation of ϕ_{FB} obtained from five different experimental tests.

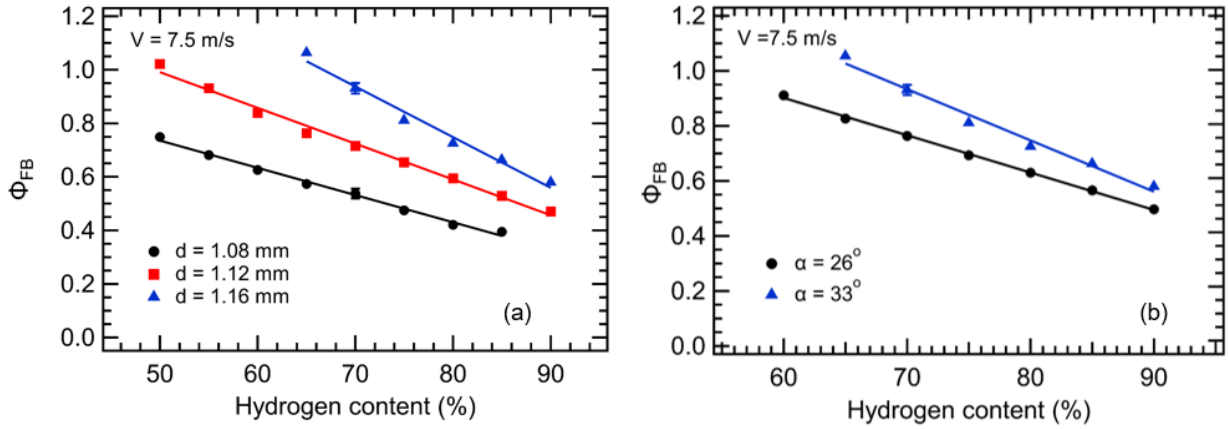

Figure 11: ϕ_{FB} as a function of X_{H_2} at V = 7.5 m/s for (a) three different perforated plate hole diameters, (b) two different swirler vane angles.

CONCLUSIONS

In this study, a ns-pulsed OH-PLIF diagnostic technique was applied to visualize stabilized flame dynamics and flashback phenomena in a premixed LSB configuration at atmospheric temperature and pressure conditions. The inlet fuel-air mixtures were varied systematically with respect to ϕ, X_{H_2} in a hydrogen-methane mixture (50%–90%), and pre-mixer velocities and the experiments were performed on a burner modified to provide optical access to the premixing section. The burner was operated in stable flame configuration and detailed investigations on the effects of different parameters on flame lift-off length were performed. The lift-off length measurement via averaged OH-PLIF images recorded at 20 kHz repetition

rate showed dependence on each of these parameters and hence OH fluorescence emission near 309 nm provides an excellent marker of the L. Flashback ϕ showed an expected linearly increasing trend with increasing pre-mixer velocities and decreasing X_{H_2} and the conclusions drawn aligned well with the detailed L investigation performed in the stabilized flame configuration. In flashback mode, the flame propagated further upstream into the pre-mixer tube and was anchored on the tip of the center-body within 30-40 ms of the entrance where flame holding occurred forming the distorted conical flame front. Such flame flashback events and other flame characteristics like local ignition, local extinction, flame curvature, local hot pockets as well as the main reaction zone of the combustion region were well characterized. Spatially and temporally resolved kHz-rate OH-PLIF is a promising technique to observe rapidly occurring flashback events and it can be applied to validate turbulence-chemistry interaction models of swirling flames. The fundamentals of flashback and a detailed picture of flashback and flame holding of hydrogen-enriched low-swirl flames was presented in this study. The insights gained by these studies can be augmented by computational fluid dynamics simulations or simultaneous velocimetry and PLIF diagnostics which are the subject of future studies.

ACKNOWLEDGMENTS

This work was performed in support of the U.S. Department of Energy's (DOE) Fossil Energy and Carbon Management's Hydrogen Combustion Research Program and executed through the National Energy Technology Laboratory (NETL) Research & Innovation Center's Turbines Field Work Proposal. The authors acknowledge the contribution of Matthew Searle for his valuable input during burner design, modification, and operation.

DISCLAIMER

This project is funded by the United States Department of Energy, National Energy Technology Laboratory, in part, through a site support contract. Neither the United States Government nor any agency thereof, nor any of their employees, nor the support contractor, nor any of their employees, makes any warranty, express or implied, or assumes any legal liability or responsibility for the accuracy, completeness, or usefulness of any information, apparatus, product, or process disclosed, or represents that its use would not infringe privately owned rights. Reference herein to any specific commercial product, process, or service by trade name, trademark, manufacturer, or otherwise does not necessarily constitute or imply its endorsement, recommendation, or favoring by the United States Government or any agency thereof. The views and opinions of authors expressed herein do not necessarily state or reflect those of the United States Government or any agency thereof.

REFERENCES

1. Chapman, A., Itaoka, K., Farabi-Asl, H., Fujii, Y., and Nakahara, M. "Societal penetration of hydrogen into the future energy system: Impacts of policy, technology and carbon targets," *International Journal of Hydrogen Energy* Vol. 45, No. 7, 2020, pp. 3883-3898.
doi: https://doi.org/10.1016/j.ijhydene.2019.12.112
2. Cecere, D., Giacomazzi, E., and Ingenito, A. "A review on hydrogen industrial aerospace applications," *International Journal of Hydrogen Energy* Vol. 39, No. 20, 2014, pp. 10731-10747.
doi: https://doi.org/10.1016/j.ijhydene.2014.04.126
3. Ball, M., and Wietschel, M. "The future of hydrogen – opportunities and challenges," *International Journal of Hydrogen Energy* Vol. 34, No. 2, 2009, pp. 615-627.
doi: https://doi.org/10.1016/j.ijhydene.2008.11.014

4. Krishnan Unni, J., Govindappa, P., and Das, L. M. "Development of hydrogen fuelled transport engine and field tests on vehicles," *International Journal of Hydrogen Energy* Vol. 42, No. 1, 2017, pp. 643-651.
doi: https://doi.org/10.1016/j.ijhydene.2016.09.107
5. Verhelst, S., and Wallner, T. "Hydrogen-fueled internal combustion engines," *Progress in Energy and Combustion Science* Vol. 35, No. 6, 2009, pp. 490-527.
doi: https://doi.org/10.1016/j.pecs.2009.08.001
6. Xiao, Y., Cao, Z., and Wang, C. "Flame stability limits of premixed low-swirl combustion," *Advances in Mechanical Engineering* Vol. 10, No. 9, 2018, p. 1687814018790878.
doi: https://doi.org/10.1177/1687814018790878
7. Cheng, R. K. "Velocity and scalar characteristics of premixed turbulent flames stabilized by weak swirl," *Combustion and Flame* Vol. 101, No. 1, 1995, pp. 1-14.
doi: https://doi.org/10.1016/0010-2180(94)00196-Y
8. Cheng, R. K. "Low Swirl Combustion," *The Gas Turbine Handbook*. U.S. Department of Energy, National Energy Technology Laboratory, 2006, pp. 241 - 254.
9. Searle, M., and Strakey, P. "Flashback of Hydrogen-Methane Mistures in a Fixed-vane, Low-swirl Burner at Atmospheric Pressure," *Proceedings of ASME Turbo Expo 2023*. Boston, Massachusetts, June 26-30, 2023.
10. Luque, J., and Crosley, D. R. "LIFBASE: Database and spectral simulation program (version 1.5)," *SRI international report MP* Vol. 99, No. 009, 1999.
11. Cabra, R., Myhrvold, T., Chen, J. Y., Dibble, R. W., Karpetis, A. N., and Barlow, R. S. "Simultaneous laser raman-rayleigh-lif measurements and numerical modeling results of a lifted turbulent H2/N2 jet flame in a vitiated coflow," *Proceedings of the Combustion Institute* Vol. 29, No. 2, 2002, pp. 1881-1888.
doi: https://doi.org/10.1016/S1540-7489(02)80228-0
12. Cabra, R., Chen, J. Y., Dibble, R. W., Karpetis, A. N., and Barlow, R. S. "Lifted methane–air jet flames in a vitiated coflow," *Combustion and Flame* Vol. 143, No. 4, 2005, pp. 491-506.
doi: https://doi.org/10.1016/j.combustflame.2005.08.019
13. T, G. "Lift-off Heights and Visible Lengths of Vertical Turbulent Jet Diffusion Flames in Still Air," *Combustion Science and Technology* Vol. 41, No. 1-2, 1984, pp. 17-29.
doi: 10.1080/00102208408923819
14. Liu, G., and Wu, Y. "Lift-off height model of hydrogen autoignited flame in turbulent hot air coflow," *International Journal of Hydrogen Energy*, 2023.
doi: https://doi.org/10.1016/j.ijhydene.2023.08.099
15. Li, Z., Wang, Z., Mo, H., and Wu, H. "Effect of the Air Flow on the Combustion Process and Preheating Effect of the Intake Manifold Burner," *Energies* Vol. 15, No. 9, 2022, p. 3260.
doi: https://doi.org/10.3390/en15093260
16. Yang, L., Weng, W., Zhu, Y., He, Y., Wang, Z., and Li, Z. "Investigation of Hydrogen Content and Dilution Effect on Syngas/Air Premixed Turbulent Flame Using OH Planar Laser-Induced Fluorescence," *Processes* Vol. 9, No. 11, 2021, p. 1894.
doi: https://doi.org/10.3390/pr9111894
17. Ilbas, M., Crayford, A. P., Yılmaz, İ., Bowen, P. J., and Syred, N. "Laminar-burning velocities of hydrogen–air and hydrogen–methane–air mixtures: An experimental study," *International Journal of Hydrogen Energy* Vol. 31, No. 12, 2006, pp. 1768-1779.
doi: https://doi.org/10.1016/j.ijhydene.2005.12.007
18. "The path towards a zero-carbon gas turbine," *Hydrogen Gas Turbines*. European Turbine Network (ETN) Global, Brussels, Belgium, 2020.
19. Goldmeer, J. "Fuel flexible gas turbines as enablers for a low or reduced carbon energy ecosystem," *Electrify Europe: Vienna, Austria*, 2018.

20. Utschick, M., and Sattelmayer, T. "Flame Holding in the Premixing Zone of a Gas Turbine Model Combustor After Forced Ignition of H2–Natural Gas–Air Mixtures," *Journal of Engineering for Gas Turbines and Power* Vol. 139, No. 4, 2016.
doi: 10.1115/1.4034647
21. Ranjan, R., and Clemens, N. T. "Insights into flashback-to-flameholding transition of hydrogen-rich stratified swirl flames," *Proceedings of the Combustion Institute* Vol. 38, No. 4, 2021, pp. 6289-6297.
doi: https://doi.org/10.1016/j.proci.2020.06.017
22. Hoferichter, V., Hirsch, C., and Sattelmayer, T. "Prediction of Confined Flame Flashback Limits Using Boundary Layer Separation Theory," *Journal of Engineering for Gas Turbines and Power* Vol. 139, No. 2, 2016.
doi: 10.1115/1.4034237
23. Zhen, H. S., Cheung, C. S., Leung, C. W., and Choy, Y. S. "Effects of hydrogen concentration on the emission and heat transfer of a premixed LPG-hydrogen flame," *International Journal of Hydrogen Energy* Vol. 37, No. 7, 2012, pp. 6097-6105.
doi: https://doi.org/10.1016/j.ijhydene.2011.12.130